



Characterization and testing of silica-supported cobalt–palladium catalysts for conversion of syngas to oxygenates

Nitin Kumar, Miranda L. Smith, J.J. Spivey*

Department of Chemical Engineering, Louisiana State University, Baton Rouge, LA 70803, USA

ARTICLE INFO

Article history:

Received 7 October 2011

Revised 14 February 2012

Accepted 16 February 2012

Available online 17 March 2012

Keywords:

Cobalt

Palladium

In situ DRIFTS

CO adsorption

Syngas

FT-IR

Oxygenates

Ethanol

Modified Fischer–Tropsch catalysts

ABSTRACT

Silica-supported Co–Pd catalysts were prepared by co-impregnation using 2 wt% Pd and two different cobalt loadings: 2 wt% (2Co–2Pd) and 10 wt% (10Co–2Pd). They were characterized by ICP-OES, H₂-TPR, *in situ* XRD, DRIFTS, and activity/selectivity in CO hydrogenation. Activity/selectivity studies showed that the 10Co–2Pd catalyst is more active for CO hydrogenation with high selectivity toward hydrocarbons, while 2Co–2Pd catalyst shows higher selectivity toward oxygenates, but considerably lower overall activity. DRIFTS studies for 10Co–2Pd catalyst at 230 °C indicated that sites at which CO adsorbs linearly are the main active sites for CO hydrogenation, which leads toward formation of hydrocarbons. On the other hand, the bridged sites were found to be the main active sites for 2Co–2Pd catalyst, which leads to increased selectivity toward oxygenated compounds. The hydrogenation of CO adsorbed on these bridge sites was found to be much slower, explaining the low activity of this catalyst.

© 2012 Elsevier Inc. All rights reserved.

1. Introduction

Research on alternative energy has become more important in recent times due to continued depletion of conventional energy resources and climbing crude oil prices. Oxygenated compounds, such as ethanol, are promising alternative fuels because of their biodegradability and renewability [1].

A viable route for the production of ethanol is the catalytic conversion of synthesis gas, which can be obtained by several means including coal gasification, natural gas, or a renewable resource like biomass [2–5]. The mechanism leading to ethanol formation requires CO to adsorb on the catalyst surface both, associatively and dissociatively. The CO insertion mechanism is proposed by many researchers [4,6–8] as the key step leading to the formation of oxygenated compounds. It is proposed that the hydrocarbon chain propagation involves stepwise addition of CH_x-monomeric units. Alternatively, chain growth termination by CO insertion would form acyl intermediates, which can be hydrogenated to form oxygenates.

Several catalytic systems have been studied for the conversion of syngas to oxygenated compounds [8–15]. Cobalt-based catalysts

have been found to be advantageous because of their low cost, low water–gas shift activity, and high activity for CO hydrogenation [16–18]. Cobalt is a well-known Fischer–Tropsch catalyst, producing primarily long-chain hydrocarbons through CO hydrogenation by C–O bond dissociation [19]. On the other hand, it is generally accepted that under conditions at which cobalt forms hydrocarbons, CO adsorption on Pd is associative (linear or multifold bridge) rather than dissociative [20–25]. For example, Poutsma et al. [24] observed the formation of methanol over supported palladium catalysts at 260–350 °C and 150–16,000 psig pressure. Addition of Pd to a silica-supported cobalt catalyst has been found to promote the CO hydrogenation activity and enhance the formation of oxygenated compounds [26,27]. It would be expected for a Co–Pd system that CO adsorption takes place both associatively (on Pd) and dissociatively (on Co). Such a catalyst would therefore be more selective toward oxygenated compounds. It is critical, however, that cobalt and palladium are in close contact to facilitate the formation of C₂₊ oxygenated compounds.

The focus of the present study is on the activity and selectivity of silica-supported Co–Pd catalysts for the conversion of syngas to oxygenates. 2 wt% Pd catalysts with two cobalt loadings (2 wt% and 10 wt%) were prepared, characterized, and tested for this purpose. *In situ* diffuse reflectance infrared Fourier transform spectroscopy (DRIFTS) technique was used to probe the surface species and the active sites for CO hydrogenation on these catalysts.

* Corresponding author.

E-mail address: jjspivey@lsu.edu (J.J. Spivey).

2. Experimental

2.1. Catalyst preparation

Co–Pd/SiO₂-based catalysts were synthesized using a conventional incipient wetness impregnation method to produce two catalysts, both with 2 wt% Pd but different cobalt loadings: 2 wt% and 10 wt% (designated as 2Co–2Pd and 10Co–2Pd respectively). The SiO₂ support was obtained from Alfa Aesar (Surface Area = 300 m²/g, Pore Volume = 1 cc/g). The precursors used for cobalt and palladium were cobalt nitrate and palladium (II) 2,4-pentanedionate [Pd(CH₃COCHCOCH₃)₂] respectively. These salts were dissolved in a calculated amount of ethanol before impregnating over SiO₂. The catalysts were dried overnight at 110 °C and calcined under air for 2 h at 450 °C at a temperature ramp of 1 °C per minute.

2.2. Inductively coupled plasma-optical emission spectrometry (ICP-OES)

The bulk elemental composition was measured using a Perkin Elmer 2000 DV ICP-optical emission spectrometer. A repeat sample analysis was carried out to estimate the experimental error.

2.3. Temperature-programed reduction (TPR)

Temperature-programed reduction (TPR) profiles of the calcined catalyst were recorded using an Altamira AMI 200-R-HP unit equipped with a thermal conductivity detector (TCD). The catalyst sample was first purged in a fixed-bed micro-reactor system under flowing argon at 150 °C for 1 h to remove traces of water and then cooled to 25 °C. TPR was performed using a 10% H₂/Ar mixture at a flow rate of 50 cm³/min while the temperature was linearly ramped from 25 °C to 750 °C at 10 °C/min.

2.4. In situ X-ray diffraction (XRD)

In situ XRD experiments were carried out at Center for Nanophase Materials Sciences (CNMS) at Oak Ridge National Laboratory (ORNL). These experiments were done with PANalytical X'Pert Pro MPD X-ray diffractometer using Cu K α radiation ($\lambda = 1.5406 \text{ \AA}$). The sample was mounted in an Anton Paar XRK hot stage, which can go up to 900 °C and 10 bar pressure and has the provision for gas flow. Fresh calcined catalyst was used for the *in situ* XRD experiments.

The gases used for the experiments are the following:

1. 2% CO, 2% Ar, balance He.
2. 4% H₂, balance He.

The catalyst was crushed to fine powder (~200 mesh) before loading in the sample chamber. The sample chamber is provided with gas inlet and outlet lines. Scans were taken in flowing H₂/He (50 sccm). The time taken for one scan was approximately 30 min, and the angle was varied from 15° to 70° (step size = 0.0167113°). The catalyst was held at the intended scan temperature during the 30 min scan.

Scans were taken at room temperature, 150 °C, 200 °C, 250 °C, and 300 °C in flowing H₂/He. Between scans, the temperature was increased at a rate of 20 °C/min. Data analysis and peak identification were done using the software X'Pert HighScorePlus (v3.0).

2.5. Catalyst activity test

CO hydrogenation reactions at differential conversions were carried out in a ¼ in. glass-lined stainless steel fixed-bed micro-reactor system at different temperatures (230 °C and 270 °C) and total pressure of 10 bar. Prior to reaction, the catalyst was reduced *in situ* for

2 h at 300 °C in flowing H₂/He mixture (50% H₂). CO hydrogenation reactions were carried out with a space velocity of 24,000 scc h⁻¹ g cat⁻¹ and an H₂/CO ratio of 2:1. For these experiments, the syngas was diluted with helium to reduce heat effects within the bed and to ensure that the conversion was low enough to keep the oxygenated products in the vapor state for online GC/FID analysis. In addition, the line from the reactor exit to the sampling valve was heat traced to prevent products from condensing upstream of the GC/FID. The sampling valves are placed in an isothermal (90 °C) oven. The GC/FID system (Shimadzu GC-2014) is equipped with two thermal conductivity detectors (TCD), used to analyze CO, CO₂, and H₂. Oxygenates and hydrocarbons analysis are done using a Restek™ RT-Q Bond column (25 m) connected to the flame ionization detector (FID). Helium was used as a carrier gas for FID column and CO/CO₂ TCD column, while N₂ is used for the H₂ TCD column. The FID column oven was programed to give the best possible separation of the products without co-elution. All selectivities are reported in terms of carbon efficiency defined as:

$$\text{Selectivity of A (\%)} = \frac{n \times (C_n)_A}{\text{Total CO reacted}} \times 100$$

where n is the number of carbons in A and $(C_n)_A$ is mol fraction of A.

The GC/FID system was calibrated with standard certified gas mixtures prior to the experiment. Different levels of concentration were used for the calibration, and a curve fitting was done between the points obtained. The calibration was checked after each completed experiment to ensure the validity of the data reported.

2.6. In situ diffuse reflectance FTIR spectroscopy (DRIFTS)

FTIR spectra were collected with a Nicolet 6700 model (Thermo Scientific) spectrometer equipped with an MCT-A detector cooled by liquid nitrogen. KBr beamsplitter was used to obtain spectra in the range of 4000–650 cm⁻¹. *In situ* measurements were carried out in a specially designed environmental chamber (Harrick) equipped with a gas inlet, outlet, and a heating/cooling system. A sample holder was used to hold ~20 mg of catalyst. DRIFTS spectra were collected by using series collection for 30 min. For each spectrum, 32 scans at a resolution of 4 cm⁻¹ were used.

Before each experiment, the catalyst was heated in helium at 150 °C for 30 min to remove any moisture and gases. The catalyst was reduced by flowing a mixture of hydrogen and helium (10% H₂ in He) for 2 h at 300 °C. The cell was then flushed with helium and brought to the desired reaction temperature (230 °C and 270 °C). Backgrounds were collected at desired temperatures after the system was allowed to equilibrate for 15 min at that temperature. Difference spectra were obtained by subtracting the background from the subsequent spectra. Two series of experiments were performed at each temperature: CO adsorption and CO hydrogenation. Each series was set for 30 min and was divided into three parts. In the first part, helium was flowed for 20 s followed by flowing CO + He for 5 min in the second part. The third part consisted of flushing with helium (for CO adsorption studies) or flowing H₂ + He (for CO hydrogenation studies) for the rest of the time. 5% CO/He was used for CO adsorption and 10% H₂/He for CO hydrogenation experiments. The experiments were carried out at 230 °C and 270 °C and performed at atmospheric pressure.

3. Results and discussion

3.1. ICP-OES

The results for ICP-OES are presented in Table 1. The numbers indicate metal wt%. The metal loadings are close to their intended values.

Table 1
ICP metal analysis results for catalysts 2Co–2Pd and 10Co–2Pd.

Catalyst	Co	Pd
2Co–2Pd	1.85 ± 0.02	1.72 ± 0.06
10Co–2Pd	8.82 ± 0.3	1.70 ± 0.08

3.2. Temperature-programmed reduction

The TPR results are shown in Fig. 1. The small peak below 100 °C can be attributed to the reduction of PdO to metallic Pd. Although, the reduction of PdO normally takes place below ambient temperature [27,28], this peak shift toward higher temperature indicates a strong interaction of PdO with cobalt and/or SiO₂. Pd-containing catalysts generally show a negative peak around 80 °C, which is attributed to the decomposition of Pd hydride formed in the reduction of PdO under hydrogen before the start of ramp at room temperature [29]. The absence of negative palladium hydride peak in both the catalysts suggests that palladium strongly interacts with cobalt [27,30].

The two-step reduction of cobalt oxide is observed for 10Co–2Pd catalyst. The peak at 145 °C can be attributed to the reduction of Co₃O₄ to CoO, and the peak at 310 °C is due to CoO reduction to metallic cobalt [18,29,31]. The area of peak at 310 °C was found to be approximately four times that of the peak at 145 °C. This does not agree with the stoichiometry of reduction of these species, suggesting that some Co₃O₄ may not have reduced under the 145 °C peak, and some contribution to the peak at 310 °C could be due to reduction of Co₃O₄ phase. It is possible that some Co₃O₄ may interact with the support, thereby decreasing its reducibility.

In order to confirm this, we conducted TPR experiments on a 10 wt% Co/SiO₂ catalyst (represented as 10Co) using the same support and prepared by the same method. The two peaks around 290 °C and 320 °C correspond to the two-step reduction of Co₃O₄ → CoO → Co. The calculated area ratio of these peaks was 1:3, which corresponds to the stoichiometry of reduction of these species. The 145 °C peak is not found for this catalyst, indicating that Pd promotion increases the reducibility of the 10Co–2Pd catalyst. The TPR indicates that 10Co–2Pd catalyst behaves partly like promoted catalyst and partly like unpromoted catalyst, suggesting that some cobalt clusters are in contact with Pd, and some are not.

For 2Co–2Pd catalyst, the PdO reduction below 100 °C is similar to that of 10Co–2Pd catalyst. However, two broad peaks centered around 175 °C and 260 °C are found for the reduction of cobalt. The area ratio of these peaks is approximately 1:1, which does

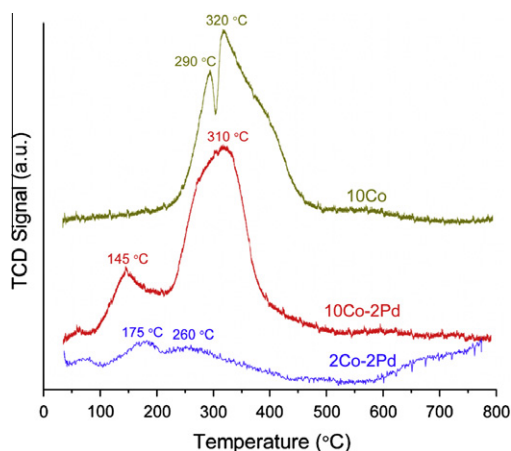


Fig. 1. Temperature-programmed reduction of cobalt-based Pd promoted and unpromoted calcined catalysts under H₂ flow.

not correspond to the stoichiometry of two-step reduction of cobalt oxide. It can therefore be concluded that there is a relatively intimate contact between cobalt and palladium in this catalyst, resulting in increased reducibility of cobalt.

3.3. In situ X-ray diffraction (XRD)

The results of *in situ* XRD for 2Co–2Pd and 10Co–2Pd catalysts are presented in Figs. 2 and 3, respectively. These experiments were conducted under flowing H₂/He at selected temperatures.

For the case of 2Co–2Pd catalyst (Fig. 2), the cobalt oxide phase is not observed, indicating that it is well dispersed. Typically, cobalt oxide usually becomes more difficult to reduce as dispersion increases [16,32]. In spite of that, the increased reducibility of this catalyst compared to 10Co–2Pd catalyst (see Fig. 1) shows the promoting effects of Pd in close contact with cobalt oxide. The PdO phase, found at 30 °C, converts to metallic Pd at 150 °C. This is consistent with the TPR, where the reduction of PdO takes place below 100 °C.

For the case of 10Co–2Pd catalyst (Fig. 3), both Co₃O₄ and PdO phases are observed at 30 °C. The crystalline PdO converts to metallic Pd by 150 °C, consistent with the TPR results. Also, CoO phase appears at 150 °C and its peak intensity increases with increasing temperature before CoO starts to convert to metallic cobalt. The presence of both, CoO and Co₃O₄ phases at 150 °C

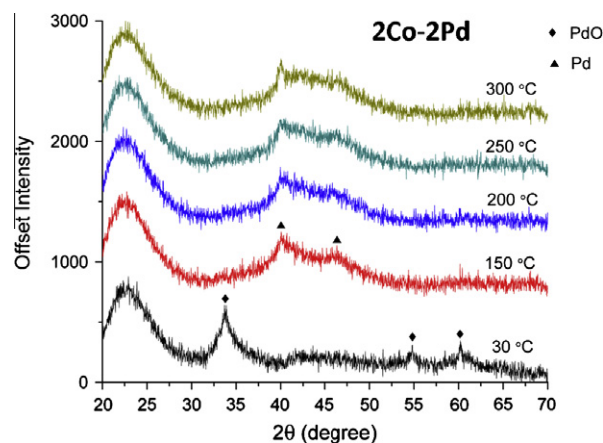


Fig. 2. *In situ* XRD results for 2Co–2Pd catalyst at different temperatures under H₂/He flow and atmospheric pressure.

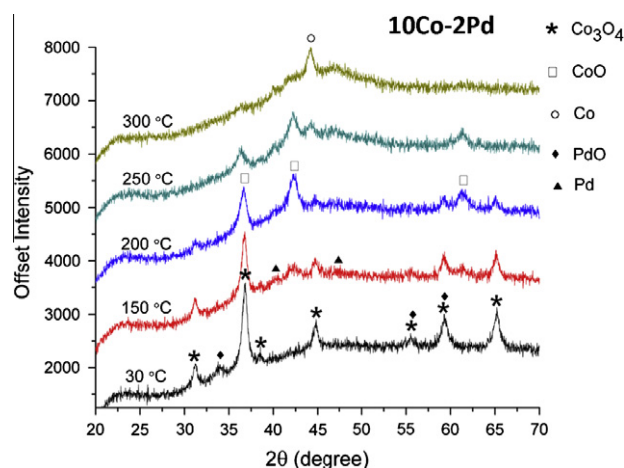


Fig. 3. *In situ* XRD results for 10Co–2Pd catalyst at different temperatures under H₂/He flow and atmospheric pressure.

Table 2Selectivities of products of CO hydrogenation reaction at different temperatures for 2Co–2Pd and 10Co–2Pd.^a The balance selectivity for all cases is due to CO₂.

Catalyst	Temp. (°C)	EtOH %	MeOH %	CH ₄ %	C ₂₊ Oxy % ^b	C ₂₊ HC % ^c	CO conversion (%)
2Co–2Pd	230	6.6	14.9	11.7	5.3	55.1	0.05
10Co–2Pd	230	3.7	2.7	43.6	4.5	41.8	1.0
2Co–2Pd	270	5.6	18.8	41.1	3.1	25.8	0.18
10Co–2Pd	270	2.5	1.2	48.0	1.7	40.2	8.2
2Co–2Pd	230 ^d	7.3	16.7	8.9	4.6	47.6	0.05
10Co–2Pd	230 ^d	2.1	2.2	47.6	6.6	36.8	0.41

^a Pressure = 10 bar, 2H₂/CO, catalyst wt = 150 mg, space velocity = 24,000 scc h⁻¹ g cat.⁻¹. Errors in the reported values are ±5.5% within 95% confidence interval.^b Includes higher oxygenates other than methanol and ethanol.^c Includes higher hydrocarbons other than methane.^d Repeated experiment at 230 °C on the same catalyst after higher temperature experiments.

indicates that the Co₃O₄ → CoO reduction is not complete at 150 °C. This is consistent with the argument given in the TPR discussion about the limited effect of palladium promotion for this catalyst. The CoO phase is found to increase with a corresponding decrease in Co₃O₄ phase as temperature is increased to 200 °C and 250 °C. Finally, the catalyst reduces completely at 300 °C, where the metallic cobalt and Pd phases are observed.

3.4. Catalyst activity test

Both the catalysts were tested for their activity and selectivity for CO hydrogenation under similar conditions. The results are presented in Table 2.

The results show that:

- 10Co–2Pd catalyst is more active than 2Co–2Pd catalyst at all temperatures studied.
- 10Co–2Pd catalyst is more selective toward total hydrocarbons as compared to 2Co–2Pd catalyst, which is more selective toward oxygenated compounds. The methanol selectivity, in particular, is much higher on 2Co–2Pd than on 10Co–2Pd catalyst.
- The CO conversion for 10Co–2Pd decreases (1.0–0.41%) when temperature is brought back to 230 °C, while for 2Co–2Pd catalyst the corresponding CO conversion is unchanged (0.05%). The apparent deactivation of 10Co–2Pd catalyst may be attributed to the oxidation of surface cobalt that is not in contact with Pd under reaction conditions. This isolated surface cobalt can deactivate by oxidation during the reaction in the absence of spillover of H₂ from neighboring Pd to cobalt, even though the oxidation of bulk metallic cobalt to either CoO or Co₃O₄ is not thermodynamically favored under these conditions [32–34]. This oxidation can be attributed to be due to the formation of metal–oxygen bonds as a result of CO hydrogenation reactions at these conditions [33,34]. These metal–oxygen bonds are stronger than those in bulk cobalt, making the oxidation of surface cobalt possible. Another argument is that the thermodynamics can be influenced by metal–support interaction, which in turn can result in oxidation of small metal clusters under conditions where bulk metal oxidation is not possible [34].

The fact that 2Co–2Pd catalyst does not show any deactivation when the temperature is brought back to 230 °C could indicate a close contact between cobalt and Pd in this catalyst, so that the cobalt remains in the reduced state during the reaction by H₂ spillover from the neighboring Pd. This conclusion is consistent with the TPR and *in situ* XRD results and discussion.

Fig. 4a and b shows CO conversion as a function of time at different temperatures for 10Co–2Pd and 2Co–2Pd catalysts, respectively. The initial decrease in activity for 2Co–2Pd catalyst at 230 °C (Fig. 4b) shows that the catalyst takes some time to reach steady state activity, which is unchanged after the 270 °C experi-

ment. For 10Co–2Pd catalyst at 270 °C, the activity drops significantly and continuously with time, as seen in Fig. 4a, but the product selectivities remain constant (not shown). It can be argued that the apparent deactivation of 10Co–2Pd catalyst is due to high CO conversion compared to that of 2Co–2Pd catalyst, thereby leading to more carbon deposition on the active sites of the catalyst.

The 2Co–2Pd catalyst shows constant activity at each temperature without much deactivation. This also supports the arguments given above that there is close contact between cobalt and Pd in this catalyst.

3.5. *In situ* diffuse reflectance FTIR spectroscopy (DRIFTS)

In order to understand the activity/selectivity behavior of these catalysts, *in situ* DRIFTS experiments were carried out at conditions similar to those of the CO hydrogenation reaction. Fig. 5 presents the results of CO desorption at 230 °C under helium flow for 10Co–2Pd catalyst. The catalyst surface was preadsorbed with CO at 230 °C before the helium flow (see experimental protocol).

The doublets between 2300–2400 cm⁻¹ and 2100–2200 cm⁻¹ are due to gaseous CO₂ and gaseous CO, respectively, which disappear with helium flow. The linearly adsorbed CO peak can be seen at 2049–2061 cm⁻¹. However, it cannot be concluded that CO is adsorbed solely on cobalt or Pd, because linear CO adsorption takes place on both the metals in this wavenumber range [35–40]. The peak at around 2005 cm⁻¹ can be attributed to compressed twofold bridging sites, and the peak in the wavenumber range of 1994–1909 cm⁻¹ can be due to isolated twofold bridging on Pd [36,41–45]. Finally, the peak at 1822 cm⁻¹ is due to threefold bridging on hollow Pd sites [44,46,47]. It can be seen that the peak intensity for all these adsorption sites decreases with time under helium flow.

The result of CO hydrogenation at 230 °C for 10Co–2Pd catalyst is presented in Fig. 6. The catalyst surface was preadsorbed with CO before starting H₂ flow. The peak intensity for bridging carbonyl (peak at 1984 cm⁻¹) increases initially before undergoing hydrogenation. Also, the linearly adsorbed CO (peak at 2053 cm⁻¹) disappears rapidly. It may be possible that some of the linearly adsorbed CO transforms to the bridged sites under H₂ flow, thereby increasing the intensity of bridge-type adsorbed CO at 1984 cm⁻¹. This transformation may occur as hydrogen adsorbs on sites already occupied by linear CO; the CO is then partially displaced and must bridge to a neighboring metal atom [38]. The rapid decrease in the linearly adsorbed CO population indicates that this CO undergoes hydrogenation preferentially as compared to the bridge-type adsorbed CO.

On comparing CO desorption (Fig. 5) and CO hydrogenation (Fig. 6), we see that the decrease in the peak intensity for linearly adsorbed CO (peak at 2053 cm⁻¹) is much faster in the case of CO hydrogenation. This can be attributed to two processes: (a) some linearly adsorbed CO transforms to bridge-type adsorbed CO and

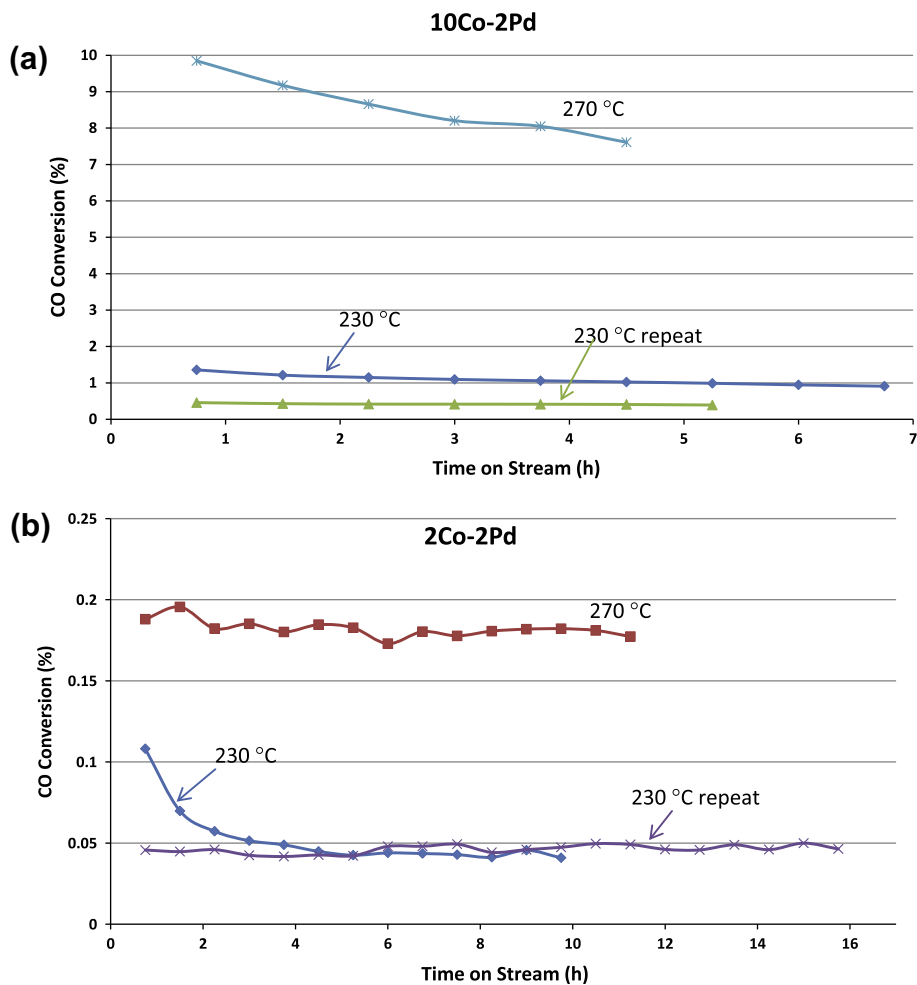


Fig. 4. CO conversion at different temperatures as a function of time for (a) 10Co-2Pd and, (b) 2Co-2Pd catalysts. The order of temperature is 230 °C → 270 °C → 230 °C repeat.

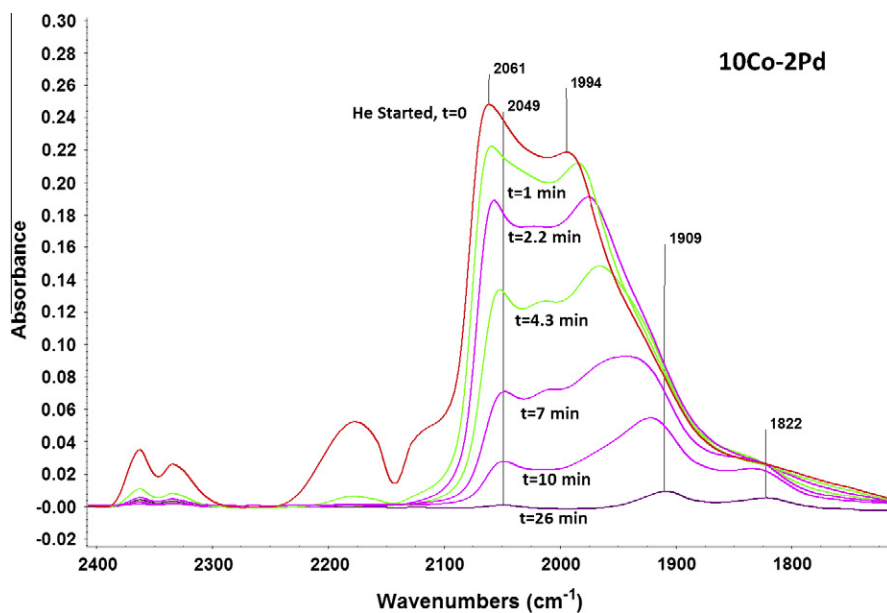


Fig. 5. CO desorption at 230 °C as a result of helium flow over 10Co-2Pd catalyst. The surface was preadsorbed with CO before starting helium flow.

(b) CO hydrogenation takes place mainly on the sites that adsorb CO linearly, thereby decreasing its peak intensity under hydrogen

flow. While the evidence of process (a) is clearly seen because the bridged CO peak intensity is increased, the much faster

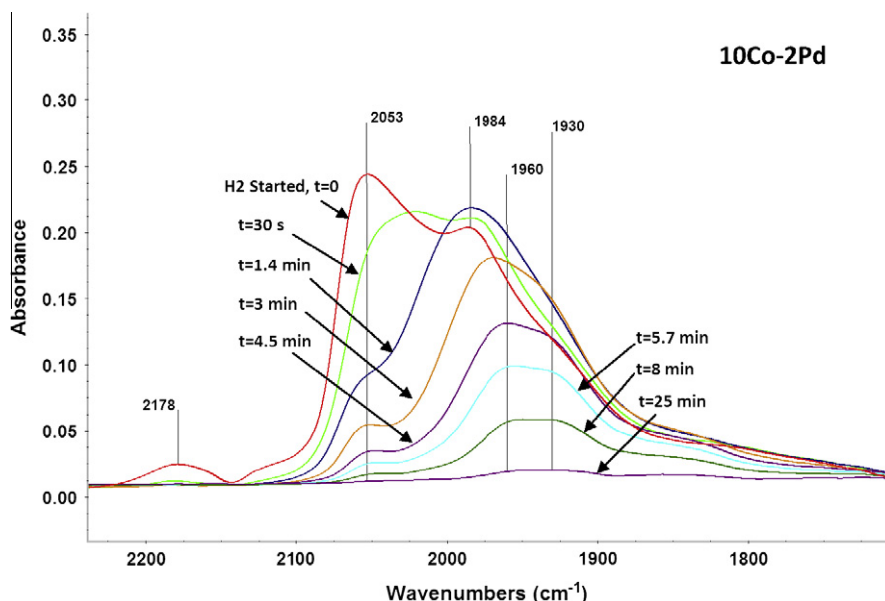


Fig. 6. CO hydrogenation at 230 °C as a result of hydrogen flow over 10Co–2Pd catalyst. The surface was preadsorbed with CO before starting hydrogen flow.

disappearance of linearly adsorbed CO peak (compare the decrease in 2053 cm^{-1} peak at $t = 0$ and $t = 1.4$ min vs. increase in 1984 cm^{-1} peak in Fig. 6) indicates that the linear sites are the most active sites for CO hydrogenation on 10Co–2Pd catalyst. Also, on comparing the 1960–1930 cm^{-1} peak intensities between $t = 5.7$ min and $t = 8$ min (when there is almost no linearly adsorbed CO left to be transformed to bridged CO) in Fig. 6, we see a relatively smaller decrease, clearly indicating that CO hydrogenation on bridged sites is much slower. Therefore, it is evident from Fig. 6 that the bridge-type adsorbed CO is less reactive to hydrogenation and is more stable than the linearly adsorbed CO.

The results for CO desorption under helium and CO hydrogenation under H_2 at 270 °C are similar to that at 230 °C, and therefore not produced here. Therefore, it can be concluded that at these temperatures linearly adsorbed CO sites are the main active site for 10Co–2Pd catalyst.

The results for CO desorption and CO hydrogenation at 230 °C for 2Co–2Pd catalyst are presented in Figs. 7 and 8, respectively.

For the case of CO desorption under helium flow (Fig. 7), we see that both linearly and bridge-type adsorbed CO peak intensities decrease with time. However, for the case of CO hydrogenation (Fig. 8), the bridge-type CO peak intensity initially increases and then the bridged species undergo hydrogenation. The site transformation from linear to bridge-type is seen here again (note the decrease in 2057 cm^{-1} peak intensity and corresponding increase in 1962 cm^{-1} peak intensity for $t = 0$ and $t = 1.2$ min in Fig. 8). However, we do not see a rapid decrease in the linearly adsorbed CO for this case, as we saw for 10Co–2Pd catalyst, suggesting that CO hydrogenation takes place on both linear and bridged sites simultaneously. But, the fact that the increase in bridged peak intensity between $t = 0$ and $t = 1.2$ in Fig. 8 is much more as compared to that between $t = 0$ and $t = 1.4$ in Fig. 6 indicates that the linearly adsorbed CO mainly transforms to bridged CO, which then undergoes hydrogenation. Therefore, it can be concluded that the active sites for 2Co–2Pd catalyst are bridge-type CO. The linearly adsorbed CO only seems to migrate to bridged sites (although some hydrogenation activity from the linearly adsorbed sites cannot be ruled out). The much larger increase in the peak area for bridged sites as compared to that of 10Co–2Pd catalyst supports this argument.

The results for CO desorption under helium and CO hydrogenation under H_2 at 270 °C are similar to that at 230 °C, and therefore not produced here. Therefore, it can be concluded that at these temperatures bridge-type adsorbed CO sites are the main active site for 2Co–2Pd catalyst.

In order to give further support to these conclusions that linear and bridged sites are the main active sites for 10Co–2Pd and 2Co–2Pd catalysts respectively, we conducted some additional experiments. These experiments were conducted on a reduced catalyst under flowing CO + H_2 gas mixture. DRIFTS spectra were collected as a function of time. The results for 10Co–2Pd and 2Co–2Pd catalysts are presented in Figs. 9 and 10, respectively.

It can be seen (Fig. 9) that the intensity of bridged sites (1984 cm^{-1}) is nearly constant till $t = 2$ min, while the intensity of linearly adsorbed CO (2054 cm^{-1}) increases slowly. The resultant peak intensity observed is due to two competing processes: (i) intensity increases with time till the steady state sites population is obtained, and (ii) adsorbed CO species undergo hydrogenation, which results in decrease in intensity. It is clear from Fig. 9 that these competing processes are taking place mostly at the linear sites on 10Co–2Pd catalyst, which results in a slower rate of increase of intensity corresponding to these sites. Thus, the argument that linear CO is the most active species is supported by this observation.

The results for the case of 2Co–2Pd catalyst (Fig. 10) are clearly in contrast to those for 10Co–2Pd catalyst. Here, we observe a slow rate of increase of bridged CO, which indicates that some of the bridged CO is undergoing hydrogenation at a rate faster than the hydrogenation of the linearly adsorbed CO. This indicates that the bridged CO is the most active species for 2Co–2Pd catalyst.

There is a disagreement in the literature about the product formation and activities from hydrogenation of linear versus bridged CO. Morales et al. [48] proposed that in the presence of hydrogen, the bridged bonded CO species hydrogenate to hydrocarbons, because the bridge-bonded CO molecule has a weaker C–O bond and thus can be more easily hydrogenated. Many other researchers [18,49,50] have concluded that the linearly adsorbed CO is the active site for the formation of oxygenated compounds, while the bridge-type adsorbed CO leads toward formation of hydrocarbon compounds. The activity of the bridge-type CO is also found to

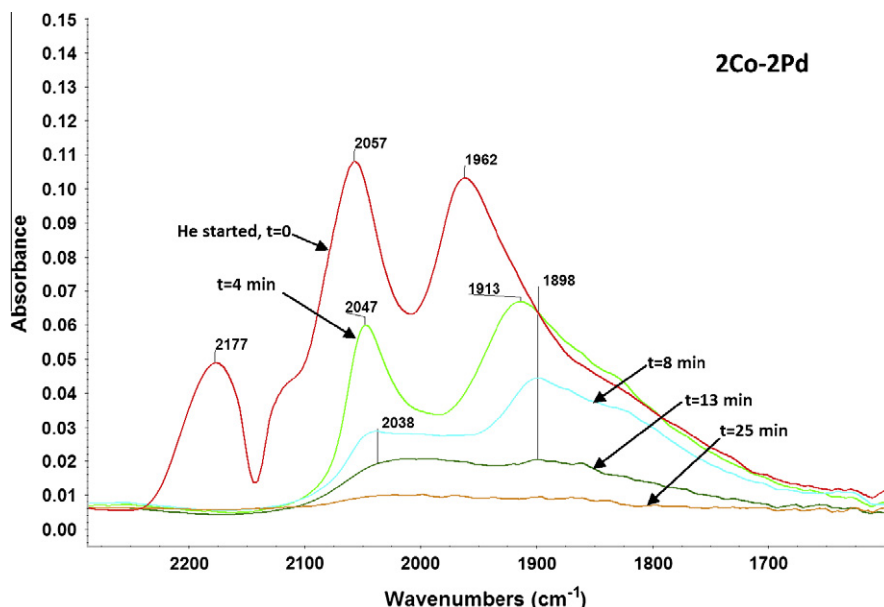


Fig. 7. CO desorption at 230 °C as a result of helium flow over 2Co–2Pd catalyst. The surface was preadsorbed with CO before starting helium flow.

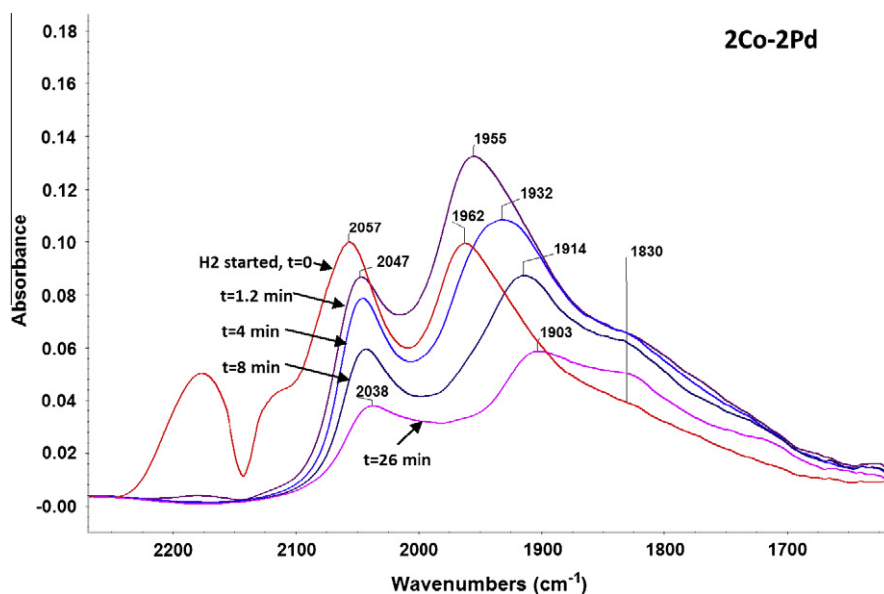


Fig. 8. CO hydrogenation at 230 °C as a result of hydrogen flow over 2Co–2Pd catalyst. The surface was preadsorbed with CO before starting hydrogen flow.

be greater than linearly adsorbed CO by these researchers. Zhang et al. [51] observed that the increase of bridged CO bands favored hydrocarbons formation and resulted in high overall CO hydrogenation activities. However, Song et al. [52] found similar activities for both, bridge-type CO and linearly adsorbed CO.

Other researchers have expressed different opinions about the activities of linear and bridge-type adsorbed CO. On a bimetallic Cu–Co catalyst, Cao et al. [53] observed only linear sites, and the bridging sites were absent. The fact that their catalyst was active toward both hydrocarbons and oxygenates led them to conclude that the ability to adsorb CO into a bridging configuration is not a prerequisite for the reactions leading to these products. Hindermann et al. [54] proposed that the first step to alcohols formation requires CO to be adsorbed in a linear or bridge form over a Cu–Co/SiO₂ catalyst, indicating that both the forms of adsorption can lead toward alcohol formation. Krishnamurthy and Chuang [55] found

linear CO to be more active than the bridged CO in the formation of methane over Rh/SiO₂ catalyst. Matsuzaki et al. [19] concluded that the formation of oxygenated compounds is favored as the ratio of bridged to linear CO species increases. Arakawa et al. [56] showed that linear CO species were responsible for high CO conversion and high selectivity toward hydrocarbons over a Co/SiO₂ catalyst prepared by using cobalt nitrate precursor. On increasing the Sr content for Re–Sr/Co(Ac)/SiO₂ catalyst, hydrocarbon formation decreased and selectivity of oxygenated compounds increased, while the CO conversion was decreased. The FT-IR results showed that with increasing Sr content, the linearly adsorbed CO decreased and bridged CO increased. Therefore, they concluded that the bridged CO is responsible for the formation of oxygenated compounds.

Our activity results (Table 2) show that 10Co–2Pd catalyst is more selective toward hydrocarbons and 2Co–2Pd catalyst is

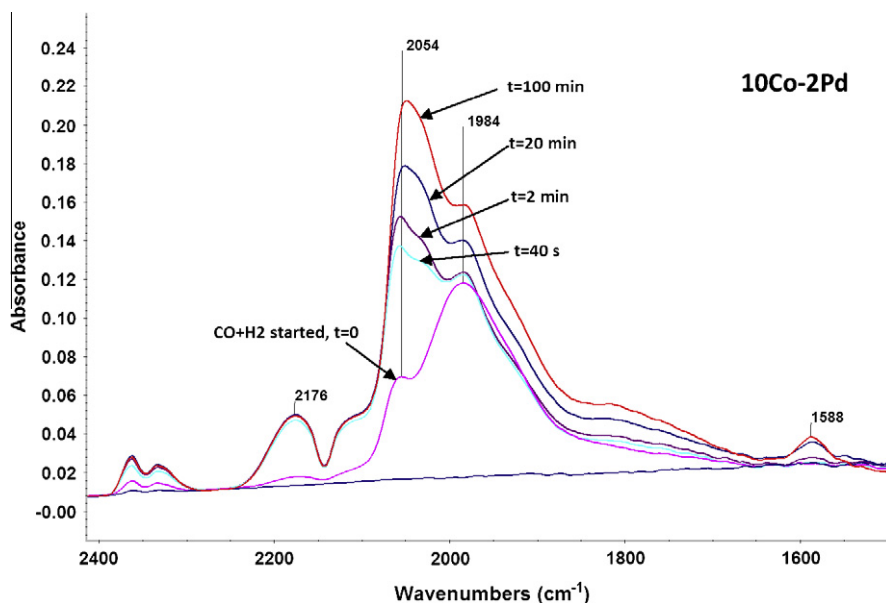


Fig. 9. CO hydrogenation at 230 °C as a result of syngas flow over reduced 10Co–2Pd catalyst.

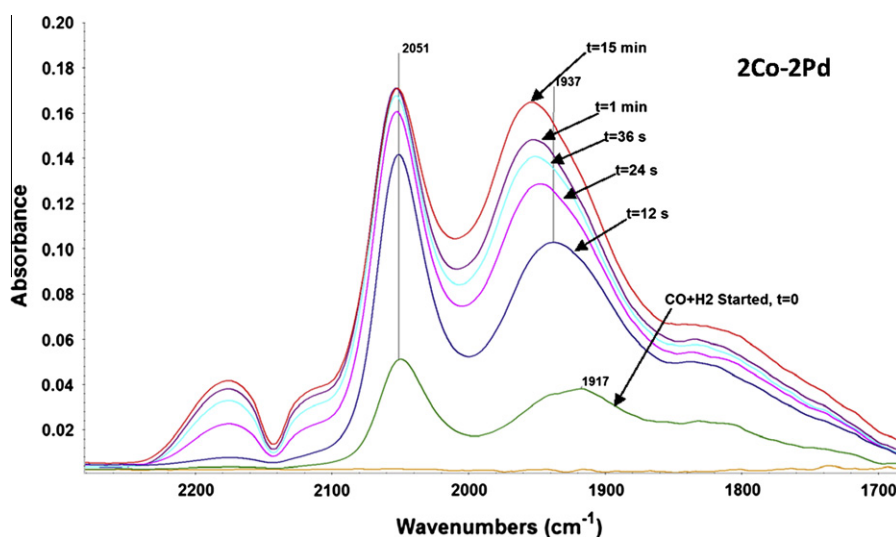


Fig. 10. CO hydrogenation at 230 °C as a result of syngas flow over reduced 2Co–2Pd catalyst.

toward oxygenated compounds. The reason for this seems to be that there are different active sites for these catalysts. The linearly adsorbed CO sites are the main active sites for CO hydrogenation for the case of 10Co–2Pd catalyst, and we believe that these sites undergo hydrogenation that leads mainly to hydrocarbon compounds. However, the bridged sites are the main active site for 2Co–2Pd catalyst, indicating that they are likelier to undergo hydrogenation to form oxygenated compounds. This raises the question: why are linear sites more active on one catalyst and bridging sites on the other? A possible answer is that the active linear sites on 10Co–2Pd catalyst consist mainly of Co sites. These highly active sites are fewer in number on 2Co–2Pd catalyst, such that the reactivity of bridge-type CO increases in a relative sense.

It is apparent that the total amount of adsorbed CO on the 10Co–2Pd catalyst, which is equivalent to the integrated area under the absorbance curve (Fig. 6), is higher than that of 2Co–2Pd catalyst (Fig. 8). The higher activity of 10Co–2Pd catalyst can also be

explained by the higher peak intensity of the active site (linearly adsorbed CO) in Fig. 6 as compared to that of the active site (bridged CO) for 2Co–2Pd catalyst (Fig. 8). The results also show that CO hydrogenation on 10Co–2Pd catalyst is much faster than on 2Co–2Pd. For example, after 25 min of hydrogen flow, the entire CO adsorbed on the catalyst surface is hydrogenated for 10Co–2Pd catalyst (Fig. 6), while for the case of 2Co–2Pd catalyst (Fig. 8), we still see a substantial population of linearly and bridge-type adsorbed CO on the surface. Earlier work on a 4.9% Pd/SiO₂ catalyst by Rabo et al. [57] indicated that CO adsorption on palladium is nondissociative, and the chemisorbed CO is less reactive to H₂ as compared to the metal-C species formed on cobalt, which is consistent with our results. Similar results were obtained at 270 °C for both the catalysts, except that the peak intensities decreased faster than that at 230 °C, indicating a higher activity at higher temperature, which is consistent with the activity results. This explains the higher activity of 10Co–2Pd catalyst as compared to 2Co–2Pd catalyst.

4. Conclusion

Silica-supported Co–Pd catalysts prepared using different cobalt loadings show different characteristics. While TPR results show an intimate contact between cobalt and palladium for the catalyst with lower cobalt loading (2Co–2Pd), the same was not true for the higher cobalt loading catalyst (10Co–2Pd). *In situ* XRD results confirmed the presence of highly dispersed cobalt for 2Co–2Pd catalyst. The addition of palladium increased the reducibility of cobalt for both the catalysts. Activity/selectivity studies on these catalysts showed contrasting behavior: 10Co–2Pd catalyst was more active but less selective toward oxygenated compounds, while 2Co–2Pd catalyst was less active and more selective toward these compounds. The hydrocarbon formation for 10Co–2Pd catalyst was significantly higher than 2Co–2Pd catalyst. 10Co–2Pd catalyst deactivated, while the 2Co–2Pd catalyst did not, probably due to close contact between cobalt and palladium in the 2Co–2Pd catalyst. The active sites for CO hydrogenation for 10Co–2Pd catalyst were those which adsorb CO linearly, while for the 2Co–2Pd catalyst the bridged sites were the main active sites leading toward the formation of oxygenated compounds.

Acknowledgments

This material is based upon work supported as part of the Center for Atomic Level Catalyst Design, an Energy Frontier Research Center funded by the US Department of Energy, Office of Science, Office of Basic Energy Sciences under Award Number DE-SC0001058. The authors are thankful to Center for Nanophase Material Sciences, which is sponsored at Oak Ridge National Laboratory by the division of Scientific User Facilities, US Department of Energy. The authors also thank Dr. Viviane Schwartz and Dr. Andrew Payzant for providing facilities for conducting *in situ* XRD experiments.

References

- [1] B.Q. He, W. Jian-Xin, J.M. Hao, X.G. Yan, J.H. Xiao, *Atmos. Environ.* 37 (2003) 949.
- [2] V. Subramani, S.K. Gangwal, *Energy Fuels* 22 (2008) 814.
- [3] A. Walter, F. Rosillo-Calle, P. Dolzan, E. Piacente, K. Borges da Cunha, *Biomass Bioenergy* 32 (2008) 730.
- [4] A. Egbibi, J.J. Spivey, *Catal. Commun.* 9 (2008) 2308.
- [5] S. Prasad, A. Singh, H.C. Joshi, *Resour. Conserv. Recycl.* 50 (2007) 1.
- [6] A. Sarkar, R.A. Keogh, S. Bao, B.H. Davis, *Appl. Catal. A* 341 (2008) 146.
- [7] J.J. Spivey, A. Egbibi, *Chem. Soc. Rev.* 36 (2007) 1514.
- [8] A.T. Bell, *React. Kinet. Catal. Lett.* 35 (1987) 107.
- [9] D.C. Koningsberger, C.P.J.H. Borgmans, A.M.J. van Elderen, B.J. Kip, J.W. Niemantsverdriet, *J. Chem. Soc. Chem. Commun.* (1987) 892.
- [10] L.M.P. van Grujthuijzen, G.J. Howsmon, W.N. Delgass, D.C. Koningsberger, R.A. van Santen, J.W. Niemantsverdriet, *J. Catal.* 170 (1997) 331.
- [11] M.M. Bhasin, W.J. Bartley, P.C. Ellgen, T.P. Wilson, *J. Catal.* 54 (1978) 120.
- [12] P.C. Ellgen, W.J. Bartley, M.M. Bhasin, T.P. Wilson, *Adv. Chem. Ser.* 178 (1979) 147.
- [13] R. Burch, M.J. Hayes, *J. Catal.* 165 (1997) 249.
- [14] J. He, W.n. Zhang, *J. Zhejiang Univ. Sci. A* 9 (2008) 714.
- [15] Y. Yang, Y. Wang, S. Liu, Q. Song, Z. Xie, Z. Gao, *Catal. Lett.* 127 (2009) 448.
- [16] A. Kababji, B. Joseph, J. Wolan, *Catal. Lett.* 130 (2009) 72.
- [17] G. Kadinov, C. Bonev, S. Todorova, A. Palazov, *J. Chem. Soc., Faraday Trans.* 94 (1998) 3027.
- [18] N. Tsubaki, S. Sun, K. Fujimoto, *J. Catal.* 199 (2001) 236.
- [19] T. Matsuzaki, K. Takeuchi, T.a. Hanaoka, H. Arawaka, Y. Sugi, *Appl. Catal. A* 105 (1993) 159.
- [20] M. Bowker, *Catal. Today* 15 (1992) 77.
- [21] P. Gelin, A.R. Siedle, J.T. Yates, *J. Phys. Chem.* 88 (1984) 2978.
- [22] W. Juszczyk, Z. Karpinski, J. Pielaszek, Z. Paal, *J. Catal.* 143 (1993) 583.
- [23] I. Matolínová, S. Fabík, K. Masek, L. Sedláček, T. Skála, K. Veltruská, V. Matolín, *Vacuum* 71 (2003) 41.
- [24] M.L. Poutsma, L.F. Elek, P.A. Ibarbia, A.P. Risch, J.A. Rabo, *J. Catal.* 52 (1978) 157.
- [25] G. Lu, T. Hoffer, L. Gucci, *Catal. Lett.* 14 (1992) 207.
- [26] K. Takeuchi, T.-a. Hanaoka, T. Matsuzaki, Y. Sugi, S. Ogasawara, Y. Abe, T. Misono, *Catal. Today* 20 (1994) 423.
- [27] C. Montes de Correa, F. Córdoba Castrillón, *J. Mol. Catal. A: Chem.* 228 (2005) 267.
- [28] V. Stonkus, K. Edolfa, L. Leite, J.W. Sobczak, L. Plyasova, P. Petrova, *Appl. Catal. A* 362 (2009) 147.
- [29] A. Sarkany, Z. Zsoldos, G. Stefler, J.W. Hightower, L. Gucci, *J. Catal.* 157 (1995) 179.
- [30] W. Juszczyk, Z. Karpinski, D. Lomot, J. Pielaszek, Z. Paal, A.Y. Stakheev, *J. Catal.* 142 (1993) 617.
- [31] A.M. Venezia, R. Murania, G. Pantaleo, V. La Parola, S. Scirè, G. Deganello, *Appl. Catal. A* 353 (2009) 296.
- [32] N. Kumar, E.A. Payzant, K. Jothimurugesan, J.J. Spivey, *Phys. Chem. Chem. Phys.* 13 (2011) 14735.
- [33] P.J. van Berge, J. van de Loosdrecht, S. Barradas, A.M. van der Kraan, *Catal. Today* 58 (2000) 321.
- [34] G. Jacobs, T.K. Das, J. Li, M. Luo, P.M. Patterson, B.H. Davis, *Stud. Surf. Sci. Catal.* 163 (2007) 217.
- [35] O. Dularent, K. Chandes, C. Bouly, D. Bianchi, *J. Catal.* 188 (1999) 237.
- [36] A. Bensalem, J.C. Muller, D. Tessier, F. Bozon-Verduraz, *J. Chem. Soc., Faraday Trans.* 92 (1996) 3233.
- [37] C.J.N.L.E.S. Rygh, *J. Catal.* 194 (2000) 401.
- [38] N. Kumar, K. Jothimurugesan, G.G. Stanley, V. Schwartz, J.J. Spivey, *J. Phys. Chem. C* 115 (2011) 990.
- [39] A. Badri, C. Binet, J.C. Lavalley, *J. Chim. Phys. Phys. – Chim. Biol.* 92 (1995) 1333.
- [40] E. Groppo, S. Bertarione, F. Rotunno, G. Agostini, D. Scarano, R. Pellegrini, G. Leofanti, A. Zecchina, C. Lamberti, *J. Phys. Chem. C* 111 (2007) 7021.
- [41] L.L. Sheu, Z. Karpinski, W.M.H. Sachtler, *J. Phys. Chem.* 93 (1989) 4890.
- [42] S.A. Shuichi Naito, Toshiki Kasahara, Toshihiro Miyao, *Res. Chem. Intermed.* 32 (2006) 279.
- [43] X. Xu, J. Szanyi, Q. Xu, D.W. Goodman, *Catal. Today* 21 (1994) 57.
- [44] G.C. Cabilla, A.L. Bonivardi, M.A. Baltanas, *Catal. Lett.* 55 (1998) 147.
- [45] N. Sheppard, T. Nguyen, *Adv. Infrared Raman Spectrosc.* 5 (1978) 67.
- [46] S. Bertarione, C. Prestipino, E. Groppo, D. Scarano, G. Spoto, A. Zecchina, R. Pellegrini, G. Leofanti, C. Lamberti, *Phys. Chem. Chem. Phys.* 8 (2006) 3676.
- [47] L.L. Sheu, H. Knozinger, W.M.H. Sachtler, *J. Mol. Catal.* 57 (1989) 61.
- [48] F. Morales, E. de Smit, F.M.F. de Groot, T. Visser, B.M. Weckhuysen, *J. Catal.* 246 (2007) 91.
- [49] H. Xiong, Y. Zhang, K. Liew, J. Li, *Fuel Process. Technol.* 90 (2009) 237.
- [50] H. Xiong, Y. Zhang, K. Liew, J. Li, *J. Mol. Catal. A: Chem.* 295 (2008) 68.
- [51] J. Zhang, J. Chen, J. Ren, Y. Sun, *Appl. Catal. A* 243 (2003) 121.
- [52] D. Song, J. Li, Q. Cai, *J. Phys. Chem. C* 111 (2007) 18970.
- [53] R. Cao, W.X. Pan, G.L. Griffin, *Langmuir* 4 (1988) 1108.
- [54] J.P. Hindermann, A. Deluzarche, R. Kieffer, A. Kiennemann, *Can. J. Chem. Eng.* 61 (1983) 21.
- [55] R. Krishnamurthy, S.S.C. Chuang, *Thermochim. Acta* 262 (1995) 215.
- [56] H. Arakawa, K. Takeuchi, T. Matsuzaki, Y. Sugi, *Jpn. Pet. Inst.* 31 (1988) 335.
- [57] J.A. Rabo, A.P. Risch, M.L. Poutsma, *J. Catal.* 53 (1978) 295.